Journal of Alloys and Compounds 499 (2010) 126–130

Contents lists available at ScienceDirect

Journal of Alloys and Compounds

journal homepage: www.elsevier.com/locate/jallcom

Role of PbO substitution by Bi_2O_3 on 1.47 μm luminescence properties of Tm^{3+}/Tb^{3+}-doped Bi_2O_3–GeO_2–Ga_2O_3 glass

D.M. Shi[a,b], Y.G. Zhao[b], Q. Qian[a], D.D. Chen[a], Q.Y. Zhang[a,*]

[a] MOE Key Lab of Specially Functional Materials and Institute of Optical Communication Materials, South China University of Technology, Guangzhou 510641, PR China
[b] Department of Materials Science and Engineering, Luoyang Institute of Science and Technology, Luoyang 471023, PR China

ARTICLE INFO

Article history:
Received 13 November 2009
Received in revised form 31 January 2010
Accepted 5 February 2010
Available online 23 March 2010

Keywords:
Spectroscopic properties
1.47 μm luminescence
Energy transfer
Rare-earth ions

ABSTRACT

Spectroscopic properties and energy transfer (ET) in Bi_2O_3(PbO)–GeO_2–Ga_2O_3 (BPGG) glass doped with Tm^{3+} and/or Tb^{3+} have been investigated. It is noted that the Tm^{3+} single-doped BPGG glass exhibits broad 1.47-μm fluorescence peaked at 1465 nm with a full width at half-maximum (FWHM) of ~134 nm. The incorporation of Tb^{3+} into Tm^{3+}-doped BPGG glass could significantly decrease the 1.80 μm emission intensity and enhance the intensity ratio of 1.47-μm to 1.80-μm ($I_{1.47}/I_{1.80}$), which reveals that Tb^{3+} ion can be considered to be an effective sensitizer ion on improving the 1.47-μm emission. The products of FWHM $\times \sigma_e^{peak}$ and $\tau_f \times \sigma_e^{peak}$ for the 1.47-μm fluorescence are in the range of 5.66–6.63 $\times 10^{-26}$ cm^3 and 8.76–10.02 $\times 10^{-25}$ cm^2 s. Effects of Bi_2O_3 substitution for PbO on spectroscopic properties, such as 1.47-μm emission of Tm^{3+}, Judd–Ofelt intensity parameters Ω_t (t = 2, 4, 6), and the lifetime of the $^3H_4$ level of Tm^{3+}, have also been investigated.

1. Introduction

Over the past several years rare-earth (RE) doped glasses, such as Er^{3+}, Tm^{3+}, and Ho^{3+} etc., have attracted a great deal of interest and importance due to their potential applications in optical fiber communications, lasers, display technology, and compact optic-electronics devices [1–5]. Currently Er^{3+}-doped fiber amplifier (EDFA) can be used to amplify signal in the C + L band (1530–1625 nm), while thulium ion as a dopant will make it possible to extend the communication band in the spectral range from 1450 to 1500 nm, which locates at the minimum loss window of silica based fiber (1200–1700 nm) and can realize the amplifying of S-band signal light [5–7]. However, the lifetime of the terminal $^3F_4$ level of Tm^{3+} is longer than that of the initial $^3H_4$ level for 1.47-μm emission, and the energy gap between $^3H_4$ and $^3H_5$ level is only 4300 cm^{-1} [6], so that a strong multiphonon relaxation easily happen, which make it difficult to realize the population inversion between the $^3H_4$ and $^3F_4$ [8–10]. Therefore, a technique that codoping with a deactivator ion to selectively reduce the lifetime of $^3F_4$ level is necessary and has been used to improve the intensity of 1.47-μm luminescence [8–11]. On the other hand, materials with lower phonon energy are required as a luminescent host to suppress the non-radiative loss from $^3H_4$ to $^3H_5$ level and obtain higher quantum efficiency for 1.47-μm emission. Recently glasses based on Ga_2O_3–Bi_2O_3–PbO system has attracted much interest for photo-electronic applications due to their excellent optical properties, such as the good transparency (~8 μm), the low phonon energy (~550 cm^{-1}), the high refractive index (~2.3), and the good glass stability and chemical durability [12–16].

Herein, the main objective of this work is to carry out a detailed study on photoluminescence (PL) properties of the Tm^{3+}-doped BPGG glass codoped with Tb^{3+} upon excitation of 808 nm laser diode (LD) to examine their suitability as potential 1.47 μm Tm^{3+}-doped fiber amplifier (TDFA). Furthermore, effects of Bi_2O_3 substitution for PbO on spectroscopic properties have also been investigated.

2. Experimental procedure

2.1. Glass preparation

BPGG glasses with the molar composition of $(20+x)Bi_2O_3$–$(45-x)$PbO–$20GeO_2$–$15Ga_2O_3$ (in mol%) (x = 0, 10, 25, and 45) were prepared. The starting materials were analytical-reagent chemicals of Bi_2O_3, PbO, and Ga_2O_3 (99.99%), GeO_2 (99.999%). By introducing Tm_2O_3 and Tb_4O_7 with 99.99% purity, the Tb^{3+} doping concentration was 0.0, 0.2 and 0.6 mol% respectively, while Tm^{3+} concentration was set to be 0.6 mol%. All the samples of about 15 g batches were prepared using a conventional melting–quenching method in crucible for 20 min at around 1100 °C, and then followed by a quenching in air on a stainless-steel plate. After annealing, all the glasses were optical polished and cut into the size of 20 mm × 20 mm × 2.0 mm.

2.2. Characterization and measurement

The absorption spectra were measured with a PERKIN-ELMER Lambda 900 UV-Visible-NIR spectrophotometer in the range of 400–2300 nm with the resolution of 1 nm. The fluorescence spectra in the range of 1300–2200 nm were obtained through

* Corresponding author. Tel.: +86 20 87113681.
E-mail address: qyzhang@scut.edu.cn (Q.Y. Zhang).

0925-8388/$ – see front matter © 2010 Elsevier B.V. All rights reserved.
doi:10.1016/j.jallcom.2010.02.200

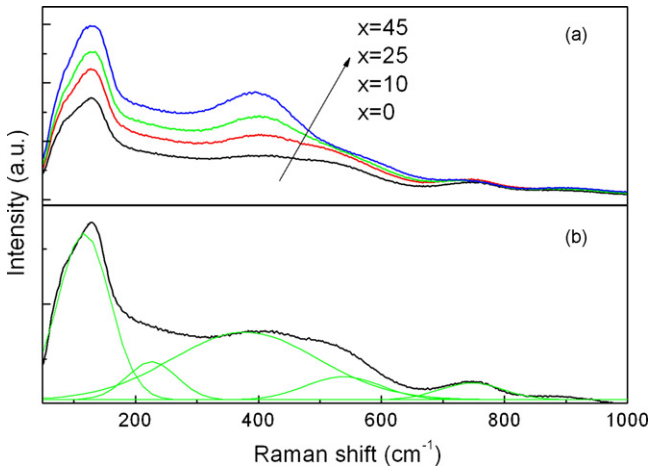

Fig. 1. (a) Raman spectra of BPGG glass with increasing the content of Bi_2O_3 substitution for PbO and (b) deconvolved Raman spectrum with fitting data of $20Bi_2O_3$–$45PbO$–$20GeO_2$–$15Ga_2O_3$ glass.

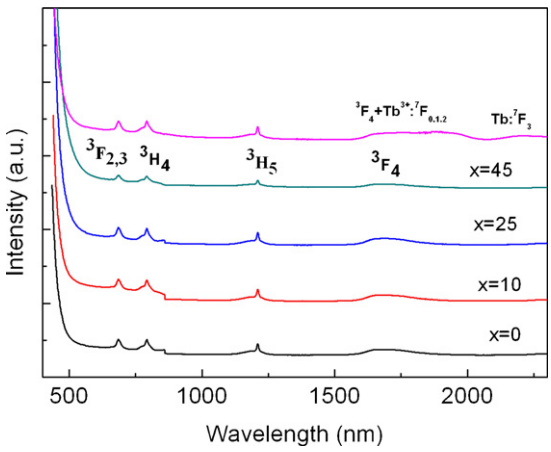

Fig. 2. Absorption spectra of Tm^{3+} and Tb^{3+} single-doped BPGG glasses (x = 0, 10, 25, and 45) and Tm^{3+}/Tb^{3+}-codoped samples, respectively. The assignments of absorption bands indicate the excited level.

a computer-controlled Triax 320 spectrofluorimeter with a 808 nm laser diode (LD), and the signal was detected with PbSe detector (1000–5000 nm) using a Stanford SR510 lock-in amplifier. Raman scattering spectra were recorded in the range of 49–1000 cm^{-1} using a microscope spectrophotometer (model RM 2000, Renishaw) with 514.5 nm laser as an excitation source and the working power is 20 mW. The fluorescence lifetimes of $^3H_4$ level were obtained from the decay curves of the Tm^{3+}: $^3H_4 \rightarrow {}^3F_4$ emission by using a computer-controlled digitizing oscilloscope through InGaAs detector (800–1650 nm). The refractive indices at 632.8 nm were obtained by Metricon 2010 prism coupler.

3. Results and discussion

3.1. Raman spectra analysis

The dependence of Raman spectra of BPGG glass on the content of Bi_2O_3 instead of PbO and the deconvolution of Raman spectrum of BPGG glass (x = 0) is shown in Fig. 1(a) and (b), respectively. The spectra contain five bands peaking at 131, 229, 385, 542, and 748 cm^{-1}, respectively. The spectra region can be classified into three main spectral regions: (1) low-frequency region $\leq$250 cm^{-1}, ascribed to the collective modes of local structures and heavy-metal ion vibrations at 120–140 cm^{-1}. The peak centered at 131 cm^{-1} can be assigned to Bi–O stretching vibration and is related to the Bi^{3+} vibration in distorted BiO_6 octahedra, whose intensity increases with the increase of Bi_2O_3 content [15,16]. In addition, it should be noted that the peak centered at 131 cm^{-1} becomes broader with increasing the content of Bi_2O_3 instead of PbO because of more uniform length of Pb–O bonds for pyramidal coordinations of Pb^{2+} ions, compared with a broader distribution in the lengths of the six Bi–O bonds in BiO_6 octahedra [16]. The low-frequency band centered at 229 cm^{-1} is associated with the collective modes of local structures and heavy-metal vibrational modes. (2) Intermediate region of 300–600 cm^{-1}, assigned to the deformation of vibrational modes of glass network structure with bridge oxygen or to symmetric stretching anion motions in angularly constrained cation–anion–cation configurations [15,16]. The 385 cm^{-1} could be ascribed to a superposition of the vibrations of Bi–O–Pb, Ga–O–Pb and Ga–O–Bi bridges [16]. Further, the band associated with Ga–O–Pb and Ga–O–Bi may be because of distorted PbO_n (n = 3, 4) pyramids and BiO_6 octahedra, respectively. The 542 cm^{-1} band is ascribed to a superposition of the bending vibrations of Bi–O–Bi and Ga–O–Ga bridges between GaO_4 tetrahedra [16]. The higher frequency of the Bi–O–Bi might lead to a larger bridging angle than that of Ga–O–Ga. (3) The high frequency region ($\geq$600 cm^{-1}) is attributed to the stretching vibrational modes of the glass network former [16–18], and the 748 cm^{-1} band is the weakest band which was induced by the stretching vibration of GeO_4 tetrahedra. Additionally it should be noted that the Bi_2O_3 substitution for PbO results in the blue shift of the peak of Raman spectra and the intensities of all peaks increase. It should be noted that blue-shift region of the peak centered at 385 cm^{-1} is larger than that of other band, which fully exhibits that the Bi–O–Ga bridge induce vibrations with lower wave numbers than other cation–anion–cation bridge vibrations.

3.2. Absorption spectra and JO analysis

Fig. 2 shows the absorption spectra in the range of 400–2300 nm for Tm^{3+}/Tb^{3+}-doped samples when Tb^{3+} concentration is set to be 0.6 mol% upon the excitation of 808 nm LD. Each band assignment corresponds to the excited level of RE^{3+} ions. With increasing the Bi_2O_3 content instead of PbO, the cutoff band shifts to a longer wavelength, which might be ascribed to larger molecular weight of Bi_2O_3 leading to the lower baseband vibrational frequency than that of PbO. Five absorption bands of Tm^{3+} and two absorption bands of Tb^{3+} are observed in Fig. 2, centered at the respective wavelengths of 1669, 1206, 793, 698, 684 nm for Tm^{3+}, and 1948, 2245 nm for Tb^{3+}. Wavelengths less than 500 nm are not observed because of the intrinsic bandgap absorption in the host glass.

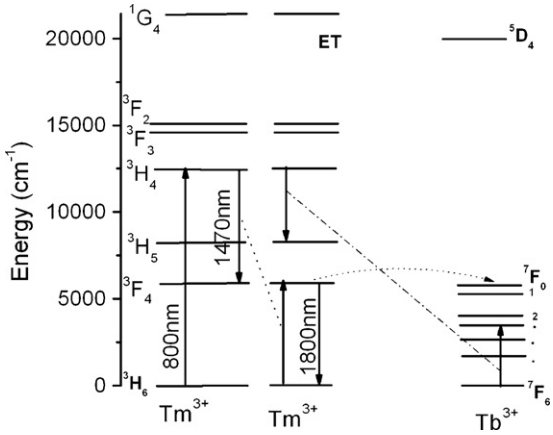

Fig. 3. Partial schematic energy level diagrams of Tm^{3+} and Tb^{3+} ions. The proposed ET routes between Tm^{3+} and Tb^{3+} are also depicted in the figure. One of the CR process among Tm^{3+} ions is also shown: $^3H_4$, $^3H_6 \rightarrow {}^3F_4$, $^3F_4$.

Fig. 3 shows partial schematic energy level diagrams of Tm^{3+} and Tb^{3+} ions. The proposed energy transfer (ET) routes from Tm^{3+} to Tb^{3+} and cross relaxation (CR) process among Tm^{3+} ion: $^3H_4$, $^3H_6 \rightarrow {}^3F_4$, $^3F_4$ are also depicted in the figure. The energy difference between the $^7F_{0,1,2}$ and $^7F_6$ states of Tb^{3+} approximately coincides with that between $^3F_4$ and $^3H_6$ states of Tm^{3+}, which makes it possible to consider Tb^{3+} as a candidate codopant. The primary mechanism is that Tm^{3+} excited to level $^3F_4$ transfers its energy to Tb^{3+} activating the $^7F_6 \rightarrow {}^7F_{0,1,2}$ transition while the Tm^{3+} decays itself to the ground state $^3H_6$. As a consequence, the population of Tm^{3+} at $^3F_4$ level decrease and the1.47-μm luminescence originated from $^3H_4 \rightarrow {}^3F_4$ transition is much easy to be emitted.

The JO theory has been substantially described in Refs. [17,18] and often employed to calculate the spectroscopic parameters, such as intensity parameters Ω_t (t = 2, 4, 6), spontaneous emission probability, branching ratio, and radiative lifetime, of RE^{3+} ions in various matrixes. The line strengths of an electric-dipole transition S_{ed} between two J states have been obtained by Eq. (1):

$$S_{ed} = \sum_{\lambda=2,4,6} \Omega_\lambda |\langle [\alpha SL]J||U^{(\lambda)}||[\alpha' S'L']J'\rangle|^2 \quad (1)$$

where J and J' are the total angular momentum of the initial level and the terminal level, respectively, the matrix elements $U^{(\lambda)}$ is given in Refs. [17,18]. S_{md} is the line strength for magnetic dipole transitions between J manifolds when the transitions abide by the selection rules $\Delta S = \Delta L = 0$, $\Delta J = 0, \pm 1$ in Russel–Saunders limit:

$$S_{md} = \frac{1}{4m^2c^2} |\langle [\alpha SL]J||L + 2S||[\alpha' S'L']\rangle J'|^2 \quad (2)$$

where the matrix elements $L + 2S$ is also given in Refs. [17,18].

The oscillator strength between two J states with an average frequency ν can be obtained by the following formula [10]:

$$f_{cal} = \frac{8\pi^2 m\nu}{3h(2J+1)e^2} \left[\frac{(n^2+2)^2}{9n} S_{ed} + nS_{md} \right] \quad (3)$$

where h is the Planck's constant, e is the elementary charge, m is the electron mass, and n is the refractive index. The experimental oscillator strength f_{mea} of the transition is given by the integrated absorption coefficients measured from the absorption spectra [10]:

$$f_{mea} = \frac{mc}{\pi e^2 N} \int \mu(\nu)\, d\nu \quad (4)$$

where N is the RE^{3+}-doping concentration, c is the velocity of light, and $\mu(\nu)$ is the absorption coefficient at frequency ν. Three intensity parameters Ω_t (t = 2, 4, and 6) can be obtained by the least-square fitting of Eqs. (3) and (4) [10,19].

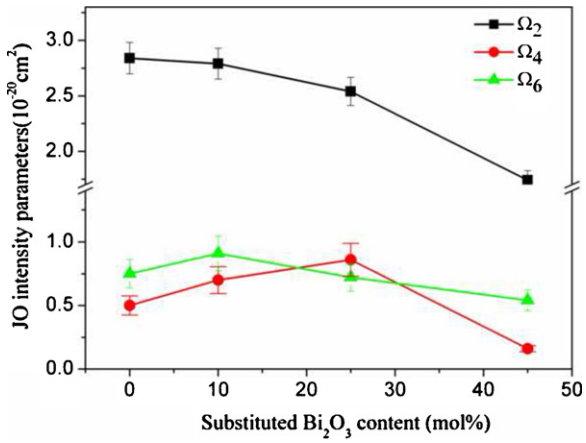

Fig. 4. Compositional dependence of intensity parameters Ω_t (t = 2, 4, 6) of Tm^{3+} single-doped BPGG (x = 0, 10, 25, and 45 mol%) glasses.

The radiative transition probabilities $A(aJ{:}bJ')$ of the different electronic transitions can be obtained from:

$$A(aJ : bJ') = A_{ed} + A_{md} = \frac{64\pi^4 e^2}{3h(2J+1)\lambda^3} \times \left[\frac{n(n^2+2)^2}{9} S_{ed}(aJ : bJ') + n^3 S_{md} \right] \quad (5)$$

where h is the Planck's constant, e is the elementary charge, n is the refractive index, and λ is the mean wavelength of the absorption band. A_{ed} and A_{md} are the radiative transition probabilities of an electric-dipole and magnetic dipole transitions, respectively.

The branching ratio β and the radiative lifetime τ_{rad} can be calculated from Eqs. (6) and (7):

$$\beta(aJ : bJ') = \frac{A(aJ : bJ')}{\sum_{bJ'} A(aJ : bJ')} \quad (6)$$

$$\tau_{rad}(J) = \frac{1}{\sum_{bJ'} A(aJ : bJ')} \quad (7)$$

The calculated Ω_t (t = 2, 4, 6) parameters of Tm^{3+} in the BPGG glasses as a function of Bi_2O_3 content are plotted in Fig. 4. With increasing Bi_2O_3 content, Ω_2 decreases monotonically while $\Omega_{4,6}$ firstly increases and then decreases. According to previous study [20], the Ω_2 parameter is sensitive to the local environment of the RE^{3+} ions and associated with covalency of the lanthanide sites, while Ω_6 parameter is related to the rigidity of the host. Higher rigidity of host matrices can be expressed by low Ω_6 values and in turn reduces the symmetry of polyhedra surrounding Tm^{3+}.

Table 1
Calculated radiative probabilities, radiative lifetimes, and branching ratios of Tm^{3+} ions in BPGG (x = 10) glass.

Transition	Average energy (cm^{-1})	A_{ed} (s^{-1})	A_{md} (s^{-1})	A (s^{-1})	β (%)	τ_{rad} (μs)
$^3F_4 \rightarrow {}^3H_6$	5881	605.971		605.972	1	1650.2
$^3H_5 \rightarrow {}^3H_6$	8247	615.445	207.276	822.722	99.34	1207.5
$\rightarrow {}^3F_4$	2366	5.428		5.428	0.66	
$^3H_4 \rightarrow {}^3H_6$	12,607	3093.867		3093.867	90.42	292.3
$\rightarrow {}^3F_4$	6726	249.556		249.556	7.29	
$\rightarrow {}^3H_5$	4360	40.846	37.307	78.153	2.29	
$^3F_3 \rightarrow {}^3H_6$	14,553	5029.324		5029.325	80.15	159.4
$\rightarrow {}^3F_4$	8672	172.495	235.907	408.403	6.51	
$\rightarrow {}^3H_5$	6305	827.776		827.776	13.19	
$\rightarrow {}^3H_4$	1945	9.107		9.107	0.15	
$^3F_2 \rightarrow {}^3H_6$	15,108	1882.649		1882.649	46.33	246.1
$\rightarrow {}^3F_4$	9227	1589.737		1589.737	39.12	
$\rightarrow {}^3H_5$	6860	552.529		552.529	13.60	
$\rightarrow {}^3H_4$	2501	38.582		38.582	0.95	
$\rightarrow {}^3F_3$	555	0.025	0.086	0.111	0.00	

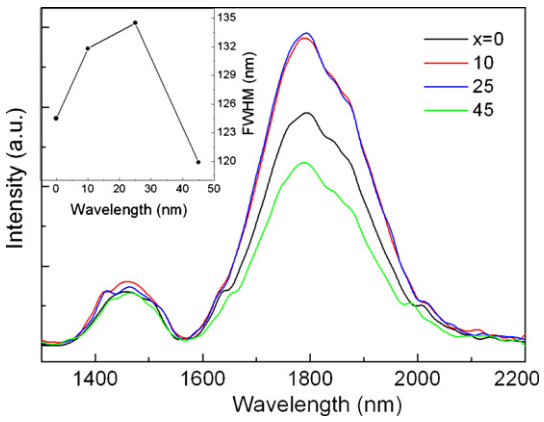

Fig. 5. Fluorescence spectra of Tm^{3+} single-doped BPGG glasses with varying the content of Bi_2O_3 substitution for PbO (x = 0, 10, 25, and 45) in the wavelength ranging 1300–2200 nm under 808 nm excitation. The inset shows the dependence of FWHM on the content of Bi_2O_3 substitution for PbO.

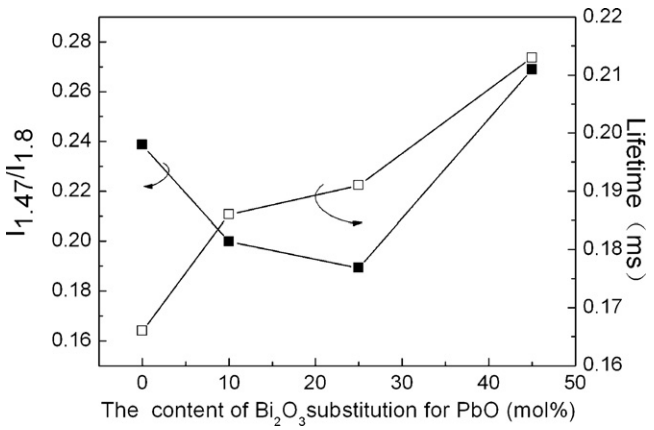

Fig. 6. Compositional dependence of the $I_{1.47}/I_{1.80}$ intensity ratio and lifetime of Tm^{3+}: $^3H_4$ level in Tm^{3+} single-doped BPGG glasses (x = 0, 10, 25, and 45 mol%).

Ω_2 value in bismuth (lead)–germanium–gallate glasses studied declines gradually from 2.84 to 1.74×10^{-20} cm^2 with increasing the Bi_2O_3 content instead of PbO, which indicates a more ionic bonding of the Tm^{3+} ions in Bi_2O_3–GeO_2–Ga_2O_3 glass than that in BPGG glass.

Table 1 shows the radiative transition probability A, the fluorescence branching ratio β and radiative lifetimes τ_{rad} of the Tm^{3+} ion at x = 10 in Tm^{3+} single-doped sample. Obviously, β of the $^3H_4 \rightarrow {}^3H_6$ and $^3H_4 \rightarrow {}^3F_4$ transition are 90.42% and 7.29%, respectively. It is noted that the former is 12 times larger than the latter, indicating that the $^3H_4 \rightarrow {}^3F_4$ transition is difficult to happen. Therefore, codoping with other RE^{3+} as sensitizers is essential to improve the 1.47 μm luminescence.

3.3. Luminescence properties

Fig. 5 illustrates emission spectra of the Tm^{3+}-doped BPGG glasses in the wavelength ranging 1300–2200 nm with increasing the content of Bi_2O_3 substitution for PbO. The emission spectra centered at around 1465 and 1800 nm correspond to the transitions of $^3H_4 \rightarrow {}^3F_4$ and $^3F_4 \rightarrow {}^3H_6$ respectively, and exhibit broad emission bands for 1.47 μm luminescence with the FWHM of ~134 nm, which is significantly broader than those of tellurite (98.5 nm) [21] and ZBLAN (76 nm) [22] glasses. This property is clearly desirable for broadband TDFA host materials. Inset of Fig. 5 shows that the FWHM of 1.47-μm emission achieve to the maximum value at x = 25. The dependence of the ratio of the 1.47-μm to the 1.80-μm emission intensity ($I_{1.47}/I_{1.80}$) and the measured lifetimes of the Tm^{3+}: $^3H_4$ level on the Bi_2O_3 content is presented in Fig. 6, respectively. It is obvious that the $I_{1.47}/I_{1.80}$ ratio reaches the minimum value at x = 25 and the lifetime of $^3H_4$ level increase from 0.166 to 0.213 ms with increasing the Bi_2O_3 content instead of PbO.

Fig. 7 depicts the emission and absorption cross-sections of RE^{3+} ions transitions: (a) Tm^{3+}: $^3F_4 \rightarrow {}^3H_6$ and (b) Tb^{3+}: $^7F_6 \rightarrow {}^7F_{0,1,2}$. The emission cross-section in Tm^{3+}-doped sample was calculated by $\sigma_e(\lambda) = [\lambda^4 A_{ed} g(\nu)]/(8\pi c n^2), g(\nu) = f(\nu)/\left[\int f(\nu)\,d\nu\right]$ according to Fuchtbauer–Ladenburg equation [23], where λ is wavelength, ν is the frequency, $f(\lambda)$ is the emission line shape function, and n and c represent the refractive index and the speed of light, respectively. A_{ed} is the $^3F_4 \rightarrow {}^3H_6$ electric-dipole transition probability deduced from the JO analysis of the absorption spectra. According to the absorption spectra, the absorption cross-section can be calculated by $\sigma_{abs}(\lambda) = 2.303 \log(I_0/I)/Nl$, where $\log(I_0/I)$, l and N represent the optical density, sample thickness, and RE^{3+}-doped concentration, respectively. As shown in Fig. 7, the spectral overlap

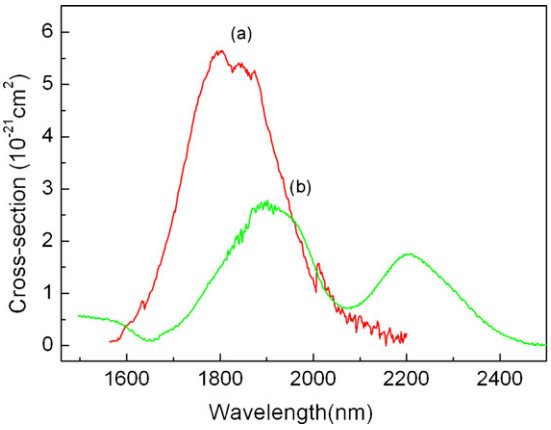

Fig. 7. Emission and absorption cross-sections of RE^{3+} ions: (a) Tm^{3+}: $^3F_4 \rightarrow {}^3H_6$ transition; (b) Tb^{3+}: $^7F_6 \rightarrow {}^7F_{0,1,2}$ transition.

between the 1.8-μm emission of Tm^{3+} and the absorption originated from $^7F_6 \rightarrow {}^7F_{0,1,2}$ transition of the Tb^{3+} ion is important and indicates the possible presence of an ET process between Tm^{3+}: $^3F_4$ level and corresponding energy level of Tb^{3+} ions. The calculated peak emission cross-section and measured lifetime is expressed as σ_e^{peak} and τ_f, respectively.

Fig. 8 shows the dependence of FWHM × σ_e^{peak} and $\tau_f \times \sigma_e^{peak}$ products of 1.47-μm luminescence on the Bi_2O_3 substitution for

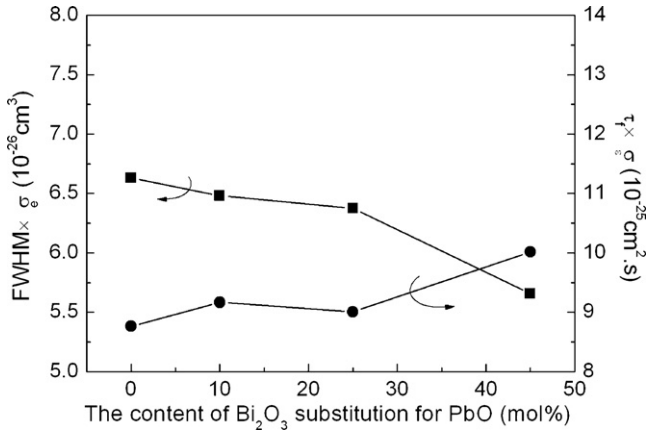

Fig. 8. The dependence of FWHM × σ_e^{peak} and $\tau_f \times \sigma_e^{peak}$ for 1.47 μm emission on the Bi_2O_3 content.

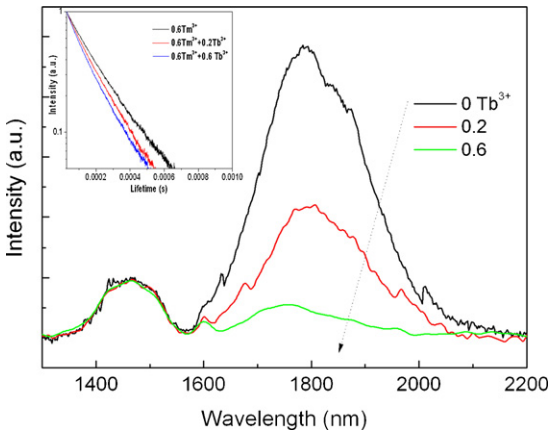

Fig. 9. Fluorescence spectra of Tm^{3+}/Tb^{3+}-doped BPGG glasses with the same Tm^{3+} concentration (0.6 mol%) in the wavelength ranging 1300–2200 nm under the excitation of 808 nm LD. The spectra are normalized to unity at the peak of the 1.47 μm. The inset shows the decay trace of the Tm^{3+}: $^3H_4$ level excited by 808 nm LD in these glasses with the increase of Tb^{3+} concentration.

PbO. The products of FWHM $\times \sigma_e^{peak}$ and $\tau_f \times \sigma_e^{peak}$ are important parameters for estimating the gain properties of TDFA. The higher products indicate the better properties. FWHM $\times \sigma_e^{peak}$ and $\tau_f \times \sigma_e^{peak}$ products of Tm^{3+}-doped BPGG glasses are in the range of 5.66–6.63 $\times 10^{-26}$ cm^3 and 8.76–10.02 $\times 10^{-25}$ cm^2 s, respectively. The values of FWHM $\times \sigma_e^{peak}$ in BPGG glasses are much higher than those of tellurite (3.339×10^{-26}) [24] and ZBLAN (1.368×10^{-26}) [25] glass. This might benefit from the higher refractive index of BPGG glasses. Additionally, it is predicted that a better gain properties of TDFA might be obtained at $x = 10$.

Fig. 9 shows emission spectra in the range of 1300–2200 nm of Tm^{3+}/Tb^{3+}-doped BPGG glasses when Tm^{3+} concentration was fixed to 0.6 mol%. The fluorescence intensities are normalized at the peak of 1.47-μm. The 1.80-μm emission intensity decreases with the increase of Tb^{3+} concentration, which indicates the ET occurs due to the well matching of resonant energies between $^3F_4$ state of Tm^{3+} and $^7F_{0,1,2}$ state of Tb^{3+}. In addition, the CR: $^3H_4$ (Tm^{3+}) + $^7F_6$ (Tb^{3+}) → $^3H_5$ (Tm^{3+}) + $^7F_3$ (Tb^{3+}) makes the population of $^3H_4$ state decrease, which is an adverse effect on the population inversion between $^3H_4$ and $^3F_4$ level of Tm^{3+}. But this is negligible in our experiment due to the rapid decrease of the 1.8-μm fluorescence originated from Tm^{3+}: $^3F_4 \rightarrow {}^3H_6$ transition with increment of the Tb^{3+} concentration, which makes the probabilities of Tm^{3+}: $^3H_4 \rightarrow {}^3H_5$ transition decline comparable to that of Tm^{3+}: $^3H_4 \rightarrow {}^3F_4$ transition. The decay traces of the Tm^{3+}: $^3H_4$ level excited by 808 nm LD in these glasses with the increase of Tb^{3+} concentration is plotted in the inset of Fig. 9. The lifetime of $^3H_4$ level slightly decrease from 0.209 to 0.149 ms, which have 28.7% of change with the increase of Tb^{3+} concentration from 0.0 to 0.6 mol%. It is reported that the lifetime of Tm^{3+} ion $^3F_4$ state can achieve 95% of reduction for incorporating Tb^{3+} comparing to that without Tb^{3+} [11]. Therefore, it is evident that Tb^{3+} can effectively improve the 1.47-μm luminescence.

4. Conclusions

In summary, we have experimentally investigated spectroscopic properties and ET of Tm^{3+}/Tb^{3+}-doped BPGG glasses under the excitation of 808 nm LD. The measured peak wavelength and the FWHM of the 1.47-μm fluorescence are 1465 and ~134 nm, respectively, in Tm^{3+} single-doped BPGG glass. The products of FWHM $\times \sigma_e^{peak}$ and $\tau_f \times \sigma_e^{peak}$ for the 1.47 μm fluorescence are in range of 5.66–6.63 $\times 10^{-26}$ cm^3 and 8.76–10.02 $\times 10^{-25}$ cm^2 s as a function of the Bi_2O_3 content instead of PbO. And the better gain properties of TDFA might be obtained when the Bi_2O_3 substitution for PbO is 10 mol%. The observed emission spectra suggest that the incorporation of Tb^{3+} into Tm^{3+}-doped BPGG glass plays a major role in decreasing the 1.80-μm fluorescence due to the ET from Tm^{3+}: $^3F_4$ to Tb: $^7F_{0,1,2}$ and increasing the 1.47-μm fluorescence. This indicates Tb^{3+} ion could be an effective sensitizer to improve the 1.47-μm fluorescence of Tm^{3+} ion. The results show that Tm^{3+}-doped BPGG glass could be suggested as promising optical materials towards the development of the 1.47-μm optical amplifier.

Acknowledgements

This work is jointly supported by the NSFC (Grant Nos. 50602017 and U0934001), the Doctorate Foundation of South China University of Technology and China Postdoctoral Science Foundation funded project.

References

[1] A.S. Gouveia-Neto, L.A. Bueno, R.F. do Nascimento, et al., Appl. Phys. Lett. 91 (2007) 091114.
[2] H. Hayashi, S. Tanabe, T. Hanada, J. Appl. Phys. 89 (2001) 1041.
[3] N.K. Giri, A.K. Singh, S.B. Rai, Spectrochim. Acta Part A 68 (2007) 117.
[4] S. Tanale, T. Kouda, T. Hanada, J. Non-Cryst. Solids 274 (2000) 55.
[5] A. Kermaoui, F. Pell'e, J. Alloys Compd. 469 (2008) 601.
[6] D.M. Shi, Q.Y. Zhang, G.F. Yang, et al., J. Non-Cryst. Solids 353 (2007) 1508.
[7] T.H. Lee, J. Heo, Y.G. Choi, et al., J. Appl. Phys. 96 (2004) 4827.
[8] Y.S. Han, J.H. Song, J. Heo, J. Am. Ceram. Soc. 87 (2004) 1381.
[9] S. Tanabe, Proc. SPIE 4282 (2001) 85.
[10] H. Yamauchi, G.S. Murugan, Y. Ohishi, J. Appl. Phys. 96 (2004) 7212.
[11] S.X. Shen, A. Jha, E. Zhang, et al., J. Lumin. 126 (2007) 434.
[12] T. Komukai, T. Yamamoto, T. Sugawa, et al., IEEE J. Quantum Electron. 31 (1995) 1880.
[13] J.E. Shelby, J. Am. Ceram. Soc. 71 (1988) C-254.
[14] D.W. Hall, A. Newhouse, N.F. Borrelli, et al., Appl. Phys. Lett. 54 (1989) 1293.
[15] Q.Y. Zhang, T. Li, Z.H. Jiang, et al., Appl. Phys. Lett. 87 (2005) 171911.
[16] F. Miyaji, S. Sakka, J. Non-Cryst. Solids 134 (1991) 77.
[17] B.R. Judd, Phys. Rev. 127 (1962) 750.
[18] G.S. Ofelt, J. Chem. Phys. 37 (1962) 511.
[19] L.R. Moorthy, T.S. Rao, K. Janardhanam, A.S. Rao, Y. Subramanyam, Opt. Mater. 12 (1999) 459.
[20] C.K. Jorgensen, R. Reisfeld, J. Less-Common Met. 93 (1983) 107.
[21] J.L. Adam, Chem. Rev. 102 (2002) 2461.
[22] A. Sennaroglu, I. Kabalci, A. Kurt, et al., J. Lumin. 116 (2006) 79.
[23] J.H. Song, J. Heo, S.H. Park, J. Appl. Phys. 93 (2003) 9441.
[24] G.F. Yang, Q.Y. Zhang, D.M. Shi, et al., Acta Phys. Sin. 55 (2006) 2613.
[25] S. Shen, M. Naftaly, A. Jha, et al., OFC (Optical Society of American, Anaheim) (2001) P. TuQ6.